Detection and Segmentation of Retinal Lesions in Retcam 3 Images Based on Active Contours Driven by Statistical Local Features

Jan KUBICEK[1], *Juraj TIMKOVIC*[2], *Marek PENHAKER*[1], *David OCZKA*[1], *Veronika KOVAROVA*[1], *Alice KRESTANOVA*[1], *Martin AUGUSTYNEK*[1], *Martin CERNY*[1]

[1]Department of Cybernetic and Biomedical Engineering, Faculty of Electrical Engineering and Computer Science, VSB–Technical University of Ostrava, 17. listopadu 15/2172, 708 33 Ostrava-Poruba, Czech Republic
[2]Clinic of Ophthalmology, University Hospital Ostrava, 17. listopadu 1790, 708 52 Ostrava-Poruba, Czech Republic

jan.kubicek@vsb.cz, timkovic.j@bluepoint.sk, marek.penhaker@vsb.cz, david.oczka@vsb.cz, veronika.kovarova.st@vsb.cz, alice.krestanova@vsb.cz, martin.augustynek@vsb.cz, martin.cerny@vsb.cz

DOI: 10.15598/aeee.v17i2.3045

Abstract. *Clinical retinal image analysis is an import aspect of clinical diagnosis in ophthalmology. Retinopathy of Prematurity (ROP) represents one of the most severe retinal disorders in prematurely born infants. One of the ROP clinical signs is the presence of retinal lesions endangering the vision system. Unfortunately, the stage and progress of these findings is often only subjectively estimated. A procedure such as this is undoubtedly linked to subjective inaccuracies depending on the experience of the ophthalmologist. In our study, a fully autonomous segmentation algorithm to model retinal lesions found using RetCam 3 is proposed. The proposed method used a combination of retinal image preprocessing and active contours for retinal lesion segmentation. Based on this procedure, a binary model of retinal lesions that allowed retinal lesions to be classified from a retinal image background was obtained. Another important aspect of the model was feature extraction. These features reliably and automatically described the development stage of an individual lesion. A complex procedure such as this has significant implications for ophthalmic clinical practice in substituting manual clinical procedures and improving the accuracy of routine clinical decisions.*

Keywords

Active contour, binary model, feature extraction, image segmentation, RetCam 3, retinal lesions.

1. Introduction

Retinal image assessment is a routine clinical procedure. Two medical imaging systems are conventionally used in the ophthalmology clinical practice. Fundus cameras, which acquire retinal images in high resolution, are used to capture individual structures in high contrast. The RetCam 3 system is used to capture retinal images with a resolution of 480×640 pixels, which is substantially lower than a fundus camera, but is, however, suitable for examinations on prematurely born children. Our research exclusively belongs to this area [1], [2], [3], [4] and [16].

When a retinal system is investigated, several major structures are important for clinical diagnosis. The center of the retina contains the optic nerve (disc), which is also a starting point for retinal blood vessels. One of the most conventional pathological findings is the retinal lesion. Such lesions are primarily a circular shape and darker intensity spectrum (Fig. 1) [5], [6], [7] and [17].

The intensity spectrum of a retinal lesion is an important feature that allows retinal lesions to be identified and also affects the effectiveness of segmentation. In some cases, the contrast in individual retinal lesions and other retinal objects is low. This low contrast is a major reason why many segmentation methods fail, because it is nearly impossible to find the edges of a retinal lesion [8], [9] and [10]. Another significant problem concerns the intensity spectrum of a retinal lesion. These spectra primarily overlap with retinal blood vessels, and it is therefore not possible

to apply the multiregional segmentation that would separate retinal lesions from the surrounding retinal structures[11], [12], [13], [14], [18] and [19].

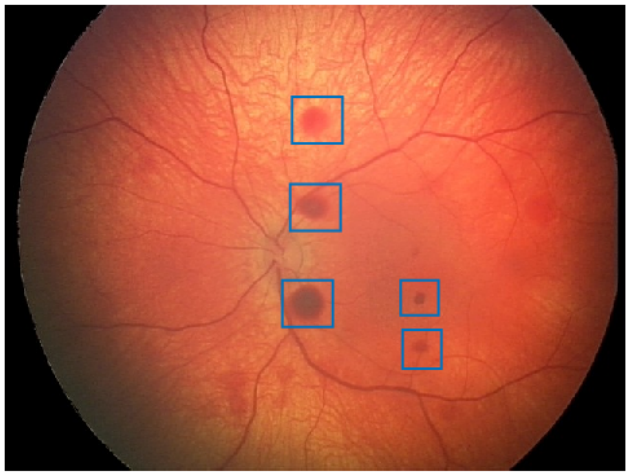

Fig. 1: A retinal image captured with RetCam 3 showing retinal lesions, indicated by the blue squares.

2. Analysis of Patient Retinal Records

For the task of segmentation and modeling retinal lesions, the University Hospital of Ostrava supplied an extensive dataset of retinal images to test the proposed segmentation model. All data was anonymized and had a unified resolution of 480×640 pixels. The quality of a certain image may depend on a physician's work with the retinal probe as well as other factors, such as observable differences in the sharpness of retinal objects and other image features. The dataset contained 2797 anonymous retinal image records. Retinal lesions were present in 1015 of these images. These images were used to test an algorithm. An example of three retinal images containing retinal lesions is shown in Fig. 2.

Fig. 2: Example from the retinal dataset showing retinal lesions.

3. Retinal Image Preprocessing

In order to enhance the features of retinal lesions, image preprocessing was applied in the algorithm to separate RGB channels, equalize histograms, and apply brightness transformation and median filtering.

First, the RGB image data was organized into individual intensity layers in order to highlight retinal lesions in each channel with the greatest contrast (Fig. 3). Empirically, a combination of the green and red channels seemed the optimal compromise. It was also apparent that retinal lesions were significantly suppressed in the blue channel.

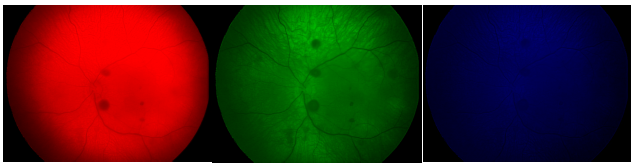

Fig. 3: RGB retinal image separated into red (left), green (middle) and blue (right) channels.

In the following step, histogram equalization was applied. This operation performs a homogenous distribution of intensity levels, which is a benefit in processing of the low-contrast data. Our procedure applied the CLAHE method (Contrast-Limited Adaptive Histogram Equalization). A distinct advantage of this method is equalization in smaller, local image segments compared to conventional histogram equalization. An example using the CLAHE method is given in Fig. 4.

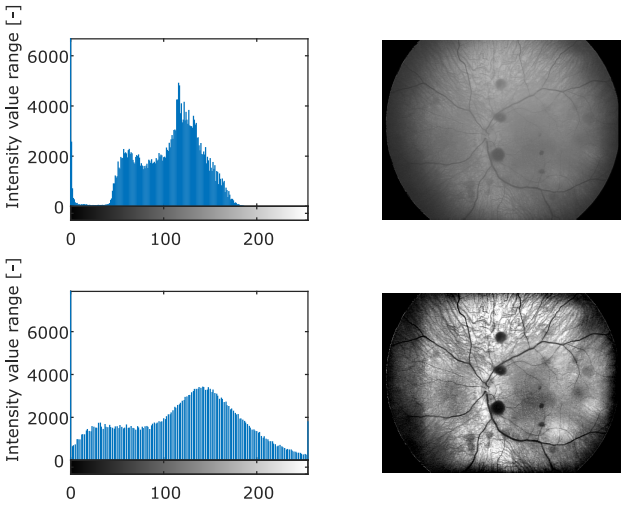

Fig. 4: Comparison of the original histogram (top) and application of the CLAHE method (bottom).

Brightness transformation was then applied. In the proposed algorithm, brightness transformation boosts the image contrast so that retinal lesions are displayed in high contrast. An example of the brightness transformation is shown in Fig. 5.

In order to prevent image noise, a median filter was applied (Fig. 6 and Fig. 7) with a 2D circular convolution and 9×9 pixel convolution kernel. Median filtering eliminated high-frequency noise, and retinal blood ves-

sels were mostly obscured from the image. This result improved the segmentation effectiveness, as the presence of blood vessels can limit segmentation accuracy because of their identical intensity spectra to retinal lesions.

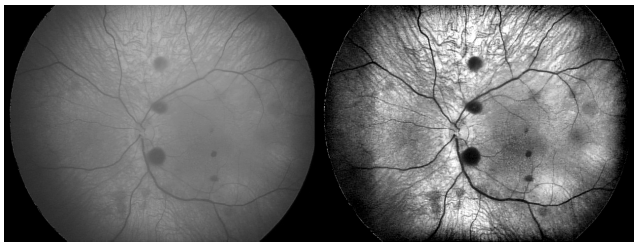

Fig. 5: Comparison of a retinal image before applying brightness transformation (left) and after brightness transformation (right).

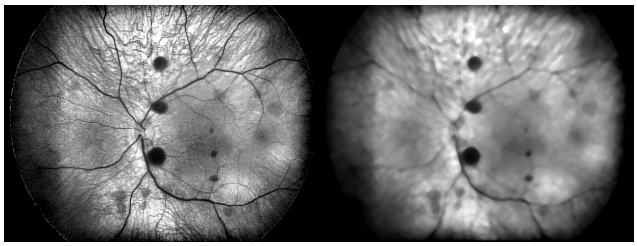

Fig. 6: A retinal image before applying median filtration (left) and after median filtration with a 9×9 kernel (right).

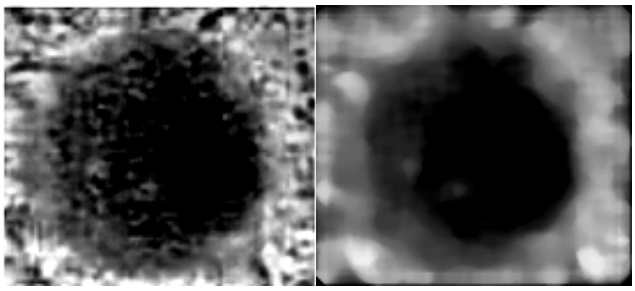

Fig. 7: Comparison of the RoI (Region of Interest) of the retinal lesion without filtration (left) and after median filtration (right).

4. Deformable Segmentation Model

In this section, a segmentation model for retinal lesions [15] is introduced. The geometrical parameters in this model can be changed according to a predefined number of segmentation steps (iterations).

We use the functional energy, representing the intensity distribution of individual pixels:

$$E^{LGDF} = \int_\Omega E_x^{LGDF} \mathrm{d}x \int_\Omega \left(\sum_{i=1}^{N} -\omega(x-y) \log p_{i,x}(I(y)) \mathrm{d}y \right) \mathrm{d}x, \tag{1}$$

where $p_{i,x}(I(y))$ represents the probability density function in the area Ω_i, $\omega(x-y)$ represents the weighted function and $-\log p$ represents the transition from minimization to the desired maximization.

It is assumed that the image region Ω can be separated into two areas: the image background and the foreground, in a form of a mathematical binary model. Using the Heaviside function H, the energy function may be expressed:

$$\begin{aligned} &E_x^{LGDF}(\phi, u_1(x), u_2(x), \sigma_1(x)^2, \sigma_2(x)^2 \\ &= -\int \omega(-y) \log p_{x,i}(I(y) M_1(\phi(y)) \mathrm{d}y \\ &-\int \omega(x-y) \log p_{x,i}(I(y) M_2(\phi(y)) \mathrm{d}y, \end{aligned} \tag{2}$$

where $M_1(\phi(y))=H(\phi(y))$ and $M_2(\phi(y))=1-H(\phi(y))$, and the energetic function can be rewritten as:

$$\begin{aligned} &E^{LGDF}(\phi, u_1, u_2, \sigma_1^2, \sigma_2^2) \\ &= \int_\Omega E_x^{LGDF}(\phi, u_1(x), u_2(x), \sigma_1^2(x), \sigma_2^2(x)) \mathrm{d}x, \end{aligned} \tag{3}$$

The level-set function is regularized in order to achieve an accurate contour evolution. This regularization prevents distortion of the active contour from the distance given:

$$P(\phi) = \int \frac{1}{2} (\mid \nabla \phi(x) \mid -1)^2 \mathrm{d}x. \tag{4}$$

The level-set function regulation is consequently done by restriction of its length:

$$L(\phi) = \int \mid \nabla H(\phi(x)) \mid \mathrm{d}x. \tag{5}$$

The entire energetic potential may be rewritten as:

$$\begin{aligned} &F(\phi, u_1, u_2, \sigma_1^2, \sigma_2^2) \\ &= E^{LGDF}(\phi, u_1, u_2, \sigma_1^2, \sigma_2^2) + \upsilon L(\phi) + \mu P(\phi), \end{aligned} \tag{6}$$

where $\upsilon, \mu > 0$ represent the weighted constants. Practically, the Heaviside function may be approximated by the smoothing function defined as:

$$H_\varepsilon = \frac{1}{2} \left[1 + \frac{1}{2} \tan^{-1} \left(\frac{x}{\varepsilon} \right) \right]. \tag{7}$$

The derivation of such a function is:

$$\delta_\varepsilon = H'_\varepsilon(x) = \frac{1}{\pi} \frac{\varepsilon}{\varepsilon^2 + x^2}. \tag{8}$$

Approximation of the energy functional is given by:

$$F(\phi, u_1, u_2, \sigma_1^2, \sigma_2^2) = E^{LGDF}(\phi, u_1, u_2, \sigma_1^2, \sigma_2^2) + \upsilon L_\varepsilon(\phi) + \mu P(\phi). \quad (9)$$

Minimization of the energy functional is done using the gradient descent flow equation:

$$\frac{\partial \phi}{\partial t} = -\delta_\varepsilon(\phi)(e_1 - e_2) + \upsilon \delta_\varepsilon(\phi) \mathrm{div}\left(\frac{\nabla \phi}{|\nabla \phi|}\right) + \mu\left(\nabla^2(\phi) - \mathrm{div}\left(\frac{\nabla \phi}{|\nabla \phi|}\right)\right), \quad (10)$$

where

$$e_1(x) = \int_\Omega \omega(y - x)\left[\log(\sigma_1(y)) + \frac{(u_1(y) - I(x))^2}{2\sigma_1(y)^2}\right] \mathrm{d}y \quad (11)$$

$$e_2(x) = \int_\Omega \omega(y - x)\left[\log(\sigma_2(y)) + \frac{(u_1(y) - I(x))^2}{2\sigma_2(y)^2}\right] \mathrm{d}y \quad (12)$$

The segmentation method is driven by controlling parameters determining the flow and smoothness of the segmentation process:

- n - the number of iterations,
- Δt - the time step of the curve shift,
- μ - a constant ensuring as minimal deviation,
- α - a constant providing weight to the image energy,
- υ - a constant affecting the contour length,
- ε - this value gives a width of the Dirac impulse, ensuring quicker movement of the initial curve,
- σ - is a parameter of the Kernel function, partially compensating for inhomogeneity of the intensity image domain,
- λ_1 - determines the weight of the area inside the curve during segmentation,
- λ_2 - determines the weight of the area outside the curve during segmentation.

5. Retinal Lesion Modeling

In this section, segmentation results and building a segmentation model are introduced. A model of a retinal lesion can be created from the initial curve traced inside a lesion. Since retinal lesions are circular in shape, a rough approximation may be done with an initial circle of smaller radius than the lesion.

A critical parameter of active contour evolution is the number of iterations. If the number of iterations was underestimated, the active contour would not reach the real borders of the lesion. However, if the segmentation process was overestimated, the segmentation curve would tend to spread outside the lesion region. We empirically set the number of iterations at 300. Figure 8 and Fig. 9 illustrate the evolution of the curve on the lesion's RoI and the entire image area, respectively.

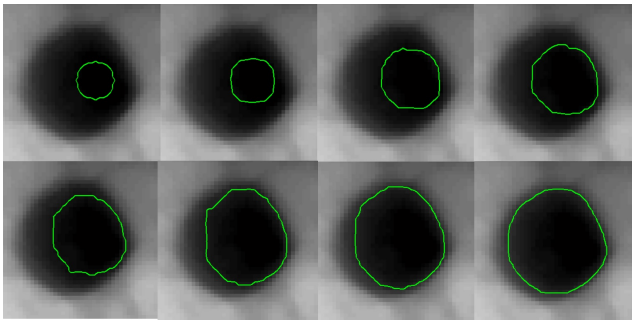

Fig. 8: Evolution of the active contour with 300 iterations on the lesion RoI.

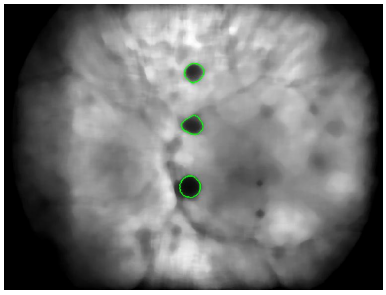

Fig. 9: Multiple detection of three retinal lesions after 300 iterations in the entire retinal image area.

The second part of the segmentation process is binarization. The area containing lesions needs to be differentiated from the image background. The evolution of an active contour is linked to the energy map. This map is able to classify the energy of the active contour. The energy inside the contour has negative energy, while the area outside has positive energy (Fig. 10). From the energy threshold, a retinal lesion model can be built (Fig. 10 and Fig. 11).

The following output (Fig. 11) shows a situation with multiple lesions present.

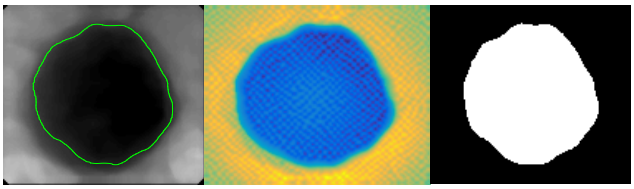

Fig. 10: Process of building a retinal lesion model: the active contour after 300 iterations (left), the energy map (center), and the binary model (right).

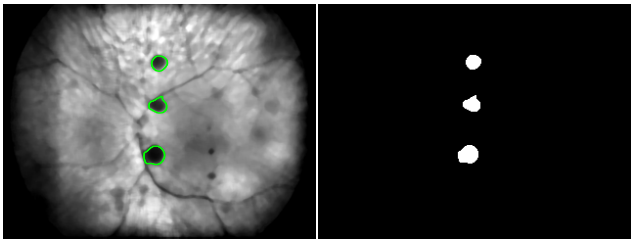

Fig. 11: A preprocessed retinal image (left) and a binary mathematical model of multiple lesions (right).

6. Tests and Quantitative Comparison

As mentioned above, the segmentation procedure depends on several aspects to determine the effectiveness and accuracy of segmentation.

The number of iterations gives information about how many times the active contour can change its shape during the segmentation process. Figure 12 shows a comparison of different iteration settings. Figure 12(a) shows that adjacent retinal blood vessels may cause significant problems when segmenting retinal lesions. If a large number of iterations is selected, the active contour tends to spread into retinal blood vessels, as their intensity spectra are nearly identical to retinal lesions.

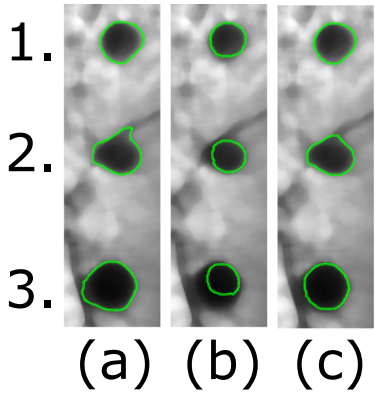

Fig. 12: Demonstration of the effect of iterations on contour modeling: (a) over-segmentation – 400 iterations, (b) under-segmentation – 50 iterations, and (c) optimal settings – 300 iterations.

The second important parameter is the size of the image matrix linked to the image features. We generally suppose that when processed retinal images have a lower resolution, the objects of interest lose their contrast, and the effect of segmentation is therefore worse. This situation can be modeled by reducing the image matrix, as shown in Fig. 13. When processing reduced images, object detail is reduced, and smoothness of the retinal lesion model is compromised.

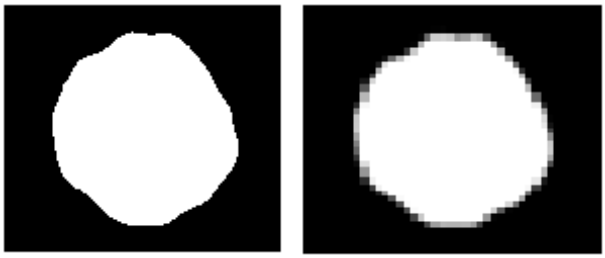

Fig. 13: Comparison of a segmentation model with 300 iterations: native retinal image data (left) and reduced image matrix, 50 % of original size (right).

As the second part of the tests, a quantitative comparison was performed. The accuracy of the proposed retinal lesion segmentation model was evaluated against conventional segmentation methods (Tab. 1). A sample of 50 retinal image records was tested in which the RoIs of the retinal lesions were extracted. The following parameters were considered in the quantitative comparison:

- **Variation of Information (*VI*)**: this parameter measures the distance between two segmentation classes C_1 and C_2 in the sense of the average conditional entropy, which is given by:

$$VI(C_1, C_2) = \mathcal{H}(C_1) + \mathcal{H}(C_2) - 2I(C_1, C_2). \quad (13)$$

- **Rand Index (*RI*)**: this parameter measures the level of similarity between the two regions. *RI* compares the compatibility of assignment between two pairs of elements in two clusters. The *RI* is given by:

$$RI(C_1, C_2) = \frac{2(n_{11} + n_{00})}{N(N-1)}, \quad (14)$$

where N denotes the total number of pixels, n_{11} is the number of pairs in the same cluster C_1 and C_2 and n_{00} is the number of pairs assigned to different clusters. *RI* has values of $[0; 1]$, where 0 indicates that the clusters are completely dissimilar, while 1 indicates that the two clusters are identical.

- **Mean Squared Error (*MSE*)**: this is an estimator measuring the average of error squares between two segmentation results. *MSE* represents a risk function that corresponds to the expected value of a squared or quadratic error loss.

- **Dice Coefficient (*DSC*)**: this parameter compares the similarity between two binary regions. When considering the binary regions X and Y, where X is the gold standard and Y is retinal lesion segmentation, the Dice Coefficient is given by:

$$DSC(X,Y) = \frac{2 \mid X \cap Y \mid}{\mid X \mid + \mid Y \mid}. \qquad (15)$$

The DSC coefficient is normalized in the range $[0;1]$, where 0 indicates no similarity, and 1 indicates a full agreement between the regions X and Y.

Tab. 1: A quantitative comparison of the proposed model with alternative segmentation methods.

	Proposed model	**Otsu**	**Fuzzy Thresholding**	**K-means clustering**	**FCM clustering**
VI	3.125	3.988	4.887	5.112	3.668
RI	0.987	0.811	0.945	0.654	0.739
MSE	33.254	45.568	44.221	40.257	34.558
DSC	0.911	0.745	0.851	0.574	0.871

Lower values indicate a better result in *VI* and *MSE*. Higher values in the *RI* indicate a greater similarity to the gold standard, which means a better result. All the comparisons were made against the gold standard, which is a manual segmentation performed by a clinical expert. Compared to the alternative methods, the proposed iteratively deformable segmentation model achieved better results. This is also due to the character of segmentation. Alternative segmentation generated multiregional segmentation in which the intensity spectra of retinal lesions partially overlapped retinal lesions. The retinal lesions were thus over-segmented when retinal blood vessels were present.

Finally, complications related to time in the proposed segmentation model were examined. The segmentation algorithm was as effective as it was time-consuming . This complication was linked to several phenomena. First, the number of iterations was a significant issue, and generally we attempted to reduce the number of iterations in order to reduce computing time. However, fewer iterations could lead to improper segmentation results. Second, image resolution affected computing time. The segmentation procedure worked more quickly on images with a lower resolution. The testing procedure was done for a selected number of iterations: 50, 150, and 300. The image matrix was concurrently reduced to 75 %, 50 %, and 40 % of the original size. Table 2 and Tab. 3 show the average results of 40 retinal images in which the most significant lesions were selected for segmentation.

Tab. 2: Time required (in seconds) for 40 retinal records with different segmentation settings. Results are averaged.

	Image resizing			
Number of iterations	100 %	75 %	50 %	40 %
50	4.32 s	3.55 s	3.12 s	2.49 s
150	12.25 s	9.44 s	8.44 s	7.63 s
300	15.95 s	11.52 s	9.25 s	8.74 s

Tab. 3: Time required (in seconds) for 40 retinal records with different segmentation settings. Results are median.

	Image resizing			
Number of iterations	100 %	75 %	50 %	40 %
50	4.12 s	3.41 s	3.74 s	2.66 s
150	12.65 s	9.84 s	9.21 s	8.44 s
300	15.41 s	12.12 s	9.47 s	8.98 s

7. Conclusion

Analysis of retinal lesions was presented in this paper. Modeling of retinal lesions has direct implications in the clinical practice of ophthalmology. Evaluating the geometrical parameters of retinal lesions in retinal images is a critical step in clinical diagnosis.

A complex segmentation method for modeling retinal lesions was proposed. First, an image preprocessing algorithm was introduced. The algorithm enhanced features in a retinal image by boosting the contrast between individual retinal lesions and the retinal image background.

The main feature of the segmentation algorithm was the deformable segmentation procedure that allowed geometrical features to be modified over time with a predefined number of iterations. Experimentally, 300 iterations were found a good compromise in terms of the algorithm's performance and time required for computing. In the final step of the segmentation procedure, a binary model of a retinal lesion was made. This model was based on the classification of the active contour's energy map.

A limitation of the model was simultaneous segmentation of multiple retinal lesions. All of these lesions would be classified into a binary model of the same class. It was therefore not possible to differentiate between individual lesions in the segmentation model. Future work will involve developing an improved model offering a classification procedure for individual retinal lesions. This method would provide tracking for discrete lesions. Using this procedure, the clinical development of individual retinal lesions could be tracked.

Acknowledgment

This work and contributions were supported by the project SV4508811/2101 Biomedical Engineering Systems XIV. This study was also supported by the Czech Science Foundation (GACR) research project 2017 No. 17-03037S Investment evaluation of medical device development run at the Faculty of Informatics and Management, University of Hradec Kralove, Czech Republic. This study was supported by the Czech Science Foundation (GACR) research project ETA No. TL01000302 Medical devices development as an efficient investment for public and private entities.

References

[1] KUBICEK, J., J. TIMKOVIC, M. PENHAKER, M. AUGUSTYNEK, I. BRYJOVA and V. KASIK. Extraction of Optical Disc Geometrical Parameters with Using of Active Snake Model with Gradient Directional Information. In: *Intelligent Information and Database Systems*. Cham: Springer, 2017, pp. 445–454. ISBN 978-3-319-54429-8. DOI: 10.1007/978-3-319-54430-4_43.

[2] MORRISON, D., E. D. BOTHUN, G. YING, E. DANIEL, A. BAUMRITTER and G. QUINN. Impact of number and quality of retinal images in a telemedicine screening program for ROP: results from the e-ROP study. *Journal of American Association for Pediatric Ophthalmology and Strabismus*. 2016, vol. 20, iss. 6, pp. 481–485. ISSN 1091-8531. DOI: 10.1016/j.jaapos.2016.08.004.

[3] BOWL, W., B. LORENZ, K. STIEGER, S. SCHWEINFURTH, K. HOLVE, C. FRIEDBURG and M. ANDRASSI-DARIDA. Correlation of central visual function and ROP risk factors in prematures with and without acute ROP at the age of 6-13 years: the Giessen long-term ROP study. *British Journal of Ophthalmology*. 2016, vol. 100, iss. 9, pp. 1238–1244. ISSN 0007-1161. DOI: 10.1136/bjophthalmol-2015-307855.

[4] KARP, K. A., A. BAUMRITTER and D. J. PEARSON. Training retinal imagers for retinopathy of prematurity (ROP) screening. *Journal of American Association for Pediatric Ophthalmology and Strabismus*. 2016, vol. 20, iss. 3, pp. 214–219. ISSN 1091-8531. DOI: 10.1016/j.jaapos.2016.01.016.

[5] RANI, P. and E. R. RAJKUMAR. Classification of retinopathy of prematurity using back propagation neural network. *International Journal of Biomedical Engineering and Technology*. 2016, vol. 22, iss. 4, pp. 338–348. ISSN 1752-6418. DOI: 10.1504/IJBET.2016.081221.

[6] SWEENEY, A. R., Q. ZHANG, R. K. WANG and K. A. REZAEI. Optical Coherence Tomography Microangiography Imaging of Circumscribed Choroidal Hemangioma. *Ophthalmic Surgery, Lasers and Imaging Retina*. 2018, vol. 49, iss. 2, pp. 134–137. ISSN 2325-8160. DOI: 10.3928/23258160-20180129-09.

[7] KAUR, J. and D. MITTAL. A generalized method for the segmentation of exudates from pathological retinal fundus images. *Biocybernetics and Biomedical Engineering*. 2018, vol. 38, iss. 1, pp. 27–53. ISSN 0208-5216. DOI: 10.1016/j.bbe.2017.10.003.

[8] TAN, J. H., H. FUJITA, S. SIVAPRASAD, S. V. BHANDARY, A. K. RAO, K. C. CHUA and U. R. ACHARYA. Automated segmentation of exudates, haemorrhages, microaneurysms using single convolutional neural network. *Information Sciences*. 2017, vol. 420, iss. 1, pp. 66–76. ISSN 0020-0255. DOI: 10.1016/j.ins.2017.08.050.

[9] SAMBATURU, B., B. SRINIVASAN, S. M. PRABHU, K. T. RAJAMANI, T. PALANISAMY, G. HARITZ and D. SINGH. A novel deep learning based method for retinal lesion detection. In: *International Conference on Advances in Computing, Communications and Informatics*. Udupi: IEEE, 2017, pp. 33–37. ISBN 978-1-5090-6367-3. DOI: 10.1109/ICACCI.2017.8125812.

[10] QU, M., C. NI, M. CHEN, L. ZHENG, L. DAI, B. SHENG, P. LI and Q. WU. Automatic diabetic retinopathy diagnosis using adjustable ophthalmoscope and multi-scale line operator. *Pervasive and Mobile Computing*. 2017, vol. 41, iss. 1, pp. 490–503. ISSN 1574-1192. DOI: 10.1016/j.pmcj.2017.04.003.

[11] KUBICEK, J., J. TIMKOVIC, A. KRESTANOVA, M. AUGUSTYNEK, M. PENHAKER and I. BRYJOVA. Morphological segmentation of retinal blood vessels and consequent tortuosity extraction. *Journal of Telecommunication, Electronic and Computer Engineering*. 2018, vol. 10, iss. 1, pp. 73–77. ISSN 2180-1843.

[12] KUBICEK, J., J. TIMKOVIC, J. SLONKA, M. PENHAKER, M. AUGUSTYNEK and I. BRYJOVA. Optical nerve segmentation using the active shape method. *Lekar a Technika*. 2016, vol. 46, iss. 1, pp. 13-20. ISSN 0301-5491.

[13] KUBICEK, J., J. TIMKOVIC, M. AUGUSTYNEK, M. PENHAKER and M. POKRYVKOVA. Optical Nerve Disc Segmentation Using Circual Integro Differencial Operator. In: *Advanced Computer and Communication Engineering Technology*. Cham:

Springer, 2016, pp. 387–396. ISBN 978-3-319-24582-9. DOI: 10.1007/978-3-319-24584-3_32.

[14] TIMKOVIC, J., J. NEMCANSKY, D. CHOLEVIK, P. MASEK, R. AUTRATA and I. KREJCIROVA. A new modified technique for the treatment of high-risk prethreshold ROP under the direct visual control of RetCam 3. *Biomedical Papers*. 2015, vol. 159, iss. 3, pp. 413–416. ISSN 1213-8118. DOI: 10.5507/bp.2015.027.

[15] WANG, L., L. HE, A. MISHRA and C. LI. Active contours driven by local Gaussian distribution fitting energy. *Signal Processing*. 2009, vol. 89, iss. 12, pp. 2435–2447. ISSN 0165-1684. DOI: 10.1016/j.sigpro.2009.03.014.

[16] MARTINEK, R., R. KAHANKOVA, J. NEDOMA, M. FAJKUS and K. CHOLEVOVA. Fetal ECG Preprocessing Using Wavelet Transform. In: *Proceedings of the 10th International Conference on Computer Modeling and Simulation*. New York: ACM Press, 2018 pp. 39–43. ISBN 978-1-450-36339-6. DOI: 10.1145/3177457.3177503.

[17] MARTINEK, R., G. RAZERA, R. KAHANKOVA and J. ZIDEK. Optimization of the Training Symbols for Minimum Mean Square Error Equalizer. In: *Advances in Intelligent Systems and Computing*. Cham: Springer, 2018, pp. 272–287. ISBN 978-3-319-60833-4. DOI: 10.1007/978-3-319-60834-1_28.

[18] MARTINEK, R., R. KAHANKOVA, J. NEDOMA, M. FAJKUS, H. NAZERAN and J. NOWAKOVA. Adaptive Signal Processing of Fetal PCG Recorded by Interferometric Sensor. In: *Advances in Intelligent Systems and Computing*. Cham: Springer, 2018, pp. 235–243. ISBN 978-3-319-68526-7. DOI: 10.1007/978-3-319-68527-4_26.

[19] SCHMID, M., F. RIGANTI-FULGINEI, I. BERNABUCCI, A. LAUDANI, D. BIBBO, R. MUSCILLO, A. SALVINI and S. CONFORTO. SVM versus MAP on Accelerometer Data to Distinguish among Locomotor Activities Executed at Different Speeds. *Computational and Mathematical Methods in Medicine*. 2013, vol. 2013, no. 343084, pp. 1–7. ISSN 1748-670X. DOI: 10.1155/2013/343084.

About Authors

Jan KUBICEK was born in Ostrava, Czech Republic. He received an M.Sc. in Biomedical Engineering in 2012 and a Ph.D. in Technical Cybernetics specializing in Biomedical Engineering in 2018. His research interests include applied image and signal processing in medicine and statistical analysis of biomedical data.

Juraj TIMKOVIC M.D., Ph.D. is the head of the Center for Children with Visual Impairment, University Hospital of Ostrava, Czech Republic and a member of the committee of the Czech Society of Pediatric Ophthalmology and Strabismus. He holds a Ph.D. in Pediatric Ophthalmology from the Masaryk University in Brno, Czech Republic. His research and publication interests include pediatric ophthalmology and neuro-ophthalmology.

Marek PENHAKER received his M.Sc. in Measurement and Control in 1996. He completed a Ph.D. in 2000 at VSB–Technical University of Ostrava in Technical Cybernetics. He has been an Associate Professor in Biomedical Engineering since 2016. His research interests include biomedical engineering, especially medical devices and home telemetry and signal processing.

David OCZKA was born in Ostrava, the Czech Republic. He received an M.Sc. in Biomedical Engineering in 2017. His research focuses on image and signal processing in medicine.

Veronika KOVAROVA was born in Trinec, Czech Republic. She received a master's degree in 2018. Her research interests include applied image processing of retinal data.

Alice KRESTANOVA was born in Opava, Czech Republic. She received a master's degree in 2018. Her research interests include applied image processing of retinal data.

Martin AUGUSTYNEK was born in Ostrava, Czech Republic. He received habilitation qualifications in Technical Cybernetics in 2017. His research focuses on special medical devices and diagnostic methods.

Martin CERNY received an M.Sc. specializing in Measurement and Control in Biomedical Engineering in 2005 and a Ph.D. in Technical Cybernetics specializing in Biomedical Engineering in 2012 from VSB–Technical University of Ostrava, Faculty of Electrical Engineering and Computer Science, Czech Republic. Today, he is an Associate Professor at VSB–Technical University of Ostrava at the Department of Cybernetics and Biomedical Engineering. He specialized in biomedical engineering, telemedicine, inertial sensors, and remote home care systems. He is responsible for living labs that focus on modern technologies for elderly and disabled persons, which is a project driven by VSB–Technical University of Ostrava.